Biomacromolecules

pubs.acs.org/Biomac

Article

Bimodal Targeting of Human Leukocytes by Fc- and CpG-Decorated Polymersomes to Tune Immune Induction

Lucille F. van Beek,*[,‖] Pascal L. W. Welzen,[‖] Lisa U. Teufel, Irma Joosten, Dimitri A. Diavatopoulos, Jan van Hest,[‖] and Marien I. de Jonge[‖]

Cite This: *Biomacromolecules* 2021, 22, 4422−4433

Read Online

ACCESS | Metrics & More | Article Recommendations | Supporting Information

ABSTRACT: The use of well-defined nanovesicles composed of amphiphilic block copolymers (polymersomes) for delivery of adjuvants and antigens is a promising strategy for vaccine development. However, the potency of nanoparticle vaccines depends on efficient interaction with and activation of cells involved in antigen presentation, which can be achieved by targeting cellular receptors. Here, we showed that the Fc fragment display on the polymersome surface resulted in markedly improved interactions with granulocytes, monocytes, and NK cells, while for "naked" polymersomes, virtually no binding to leukocytes was observed. Moreover, CpG-decorated polymersomes were found to also interact with T and/or B cells. Interestingly, whole blood stimulations with Fc fragment and CpG-decorated polymersomes induced interleukin (IL)-6, IL-8, and TNF-α production, while naked polymersomes did not induce any cytokine production. In conclusion, specific immune induction by polymersomes can be controlled using bimodal targeting of different immune receptors, which is an essential feature for targeted vaccine delivery.

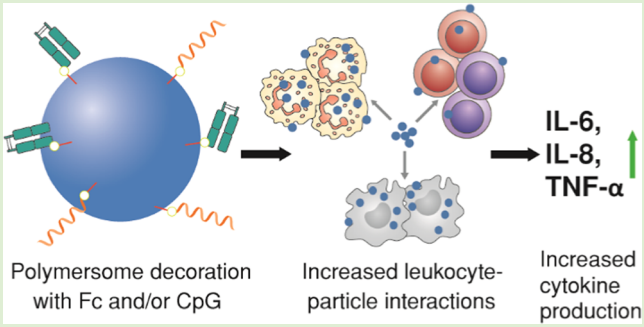

INTRODUCTION

Nanoparticles made of amphiphilic block copolymers, also known as polymersomes, represent an excellent platform for drug delivery and vaccine development, based on their chemical versatility, biocompatibility, biodegradability, and chemical and mechanical stability.[1−12] Furthermore, this platform lends itself for bio-conjugation techniques such as click chemistry, due to full chemical control over the polymer composition.[13] Next to surface display, the large aqueous polymersome core is highly suitable for the encapsulation of cargo. Particle-based vaccine formulations offer a variety of advantages over traditionally formulated soluble antigens with adjuvant, including the prevention of antigen degradation, higher antigen density, controlled and sustained cargo release, and the co-delivery of adjuvant and antigen to the same antigen-presenting cell (APC).[14]

Efficient delivery of antigen and adjuvant to immune cells of interest is key to the success of a vaccine formulation. Most polymersomes, however, have a PEGylated surface which acts as a stealthy shell, making these particles virtually inert for the human immune system.[15] Cell−particle interaction and subsequent internalization by immune cells can be initiated through multiple pathways, including Toll-like receptors (TLRs), scavenger receptors, complement receptors, chemokine, and interleukin receptors and Fc receptors (FcRs).[16] In line with this, *in vitro* and *in vivo* studies showed that the cellular uptake of nanoparticles can be improved by decorating them with receptor ligands.[17−21] Moreover, the type of ligand used determines the direction of immune cell targeting and activation of the immune system, resulting in an immunologically controllable system.[12]

Among all identified receptors, targeting FcRs, which recognize the Fc fragment of immunoglobulins, is a well-studied and promising approach to improve the potency of vaccine formulations.[22−25] Multiple studies provided evidence that parenteral immunization of mice with Fc-fusion protein antigens resulted in enhanced cellular and humoral immune responses compared to immunization with antigens lacking the Fc domain.[22−25] In the context of nanoparticles, decoration with Fc fragments has also been shown to improve particle internalization by murine macrophages.[21,26] Moreover, FcR targeting enhances transcytosis and is, therefore, especially of interest for mucosal applications.[27−33]

Besides targeting FcRs, other receptor ligands have also been widely investigated to improve nanoparticle targeting and/or its immune stimulatory capacity. CpG oligodeoxynucleotide (CpG ODN) is an example of such a ligand; it activates TLR-

Received: July 30, 2021
Revised: September 10, 2021
Published: September 23, 2021

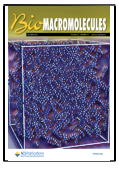

https://doi.org/10.1021/acs.biomac.1c00985
Biomacromolecules 2021, 22, 4422−4433

9, which is primarily located intracellularly in the endosomal membrane.[34,35] CpG is among the most promising adjuvants being used in humans[36] and both *in vitro* and *in vivo* studies have shown that nanoparticles in combination with CpG can successfully establish an immune response.[37−44]

The great benefit of nanoparticulate formulations is that different bioactive entities can be co-administered and displayed on the same particle scaffold. The added value of this approach has, for example, already been demonstrated by the coupling of monophosphoryl lipid A and imiquimod onto polymersomes, which resulted in the induction of immune responses against a co-delivered antigen.[45−47] In the present study, we investigated the potency and mechanism of Fc fragment- and CpG-mediated bimodal targeting in the context of polymersomes providing evidence that the simultaneous surface decoration of polymersomes with Fc fragments and CpG allows for efficient cell targeting and immune induction. This shows the potential of polymersomes as a versatile delivery system for the development of highly defined nanoparticle-based vaccines.

MATERIALS AND METHODS

Materials for Polymer and Polymersome Formation. All chemicals were used as received unless otherwise stated. Monomethoxy-poly(ethylene glycol) (PEG) (1 kDa), monoamine-PEG (1 kDa), and monoazide-PEG (3 kDa) were purchased from JenKem Technology USA. Monomer trimethylene carbonate was purchased from TCI Europe. BODIPY-FL carboxylic acid was purchased from Lumiprobe. Immunoglobulin G, Human Fc Fragment was purchased from Athenes Research Technology.

Dibenzocyclooctyne-amine-PEG_4-*N*-hydroxysuccinimide (DBCO-PEG_4-NHS) was purchased from Jena Bioscience. Amicon Ultra 0.5 mL 3 and 100 kDa spin filters were purchased from Sigma-Aldrich. CpG ODN 2006 and CpG ODN 2006-DBCO (5′ DBCO-PEG_4 modification) were purchased from Biomers.net GmbH. All other chemicals and reagents, including endotoxin-free Dulbecco's PBS (1×) (w/o Ca^{++} and Mg^{++}) were supplied by Sigma-Aldrich.

Polymer and Polymersome Characterization. *Nuclear Magnetic Resonance (NMR).* ^{1}H NMR spectra were recorded on a Bruker Avance 400 MHz spectrometer with $CDCl_3$ as a solvent and TMS as an internal standard.

Gel Permeation Chromatography (GPC). GPC was conducted using a Shimadzu Prominence GPC system with a PL gel 5 μm mixed D column (Polymer Laboratories) with a differential refractive index detector, and THF was used as an eluent with a flow rate of 1 mL/min.

Fc Fragment Concentration Measurements. Fc fragment concentrations were determined by the Pierce BCA Protein Assay according to manufacturer's instructions on a Tecan Safire II UV−Vis fluorescence and absorbance plate reader in a Greiner Flat Transparent 96-well plate (absorbance at 562 nm).

CpG ODN Concentration Measurements. CpG ODN concentrations were determined on a Thermo Scientific NanoDrop 1000 (absorbance at 280 nm).

Dynamic Light Scattering (DLS) and ζ-Potential Measurements. DLS and ζ-potential measurements were executed on a Malvern Zetasizer Nano ZSP, and the supplied software Zetasizer Software v7.13 was used for processing and analyzing the data.

Cryogenic Transmission Electron Microscopy (cryo-TEM). Experiments were performed using the CryoTitan (Thermo Fisher Scientific) equipped with a field emission gun and an autoloader and operated at a 300 kV acceleration voltage in the low-dose bright-field TEM mode. Samples for cryo-TEM were prepared by glow-discharging the grids (Lacey carbon coated, R2/2, Cu, 200 mesh, EM Sciences) in a Cressington 208 carbon coater for 40 s. Then, 4 μL of the polymersome solution was pipetted on the grid and blotted in a Vitrobot MARK III at room temperature and 100% humidity. The grid was blotted for 3 s (offset −3) and directly plunged and frozen in liquid ethane. Cryo-TEM images were acquired with the zero-loss energy filtering mode (Gatan GIF 2002, 20 eV energy slit) on a CCD camera (Gatan model 794).

Preparation of Poly(Ethylene Glycol)$_{22}$-*Block*-Poly[(ε-Caprolactone)$_{38}$-*Gradient*-(Trimethylene Carbonate)$_{37}$] (PEG-p(CL-TMC)). The block copolymer was synthesized according to a previously reported literature procedure aiming for a composition of PEG_{22}-p(CL_{35}-*g*-TMC_{35}).[3,48] A 250 mL single-neck round-bottom flask, equipped with a magnetic stir bar and an argon inlet, was charged with macroinitiator monomethoxy-PEG (M_n ∼1000 g/mol; 705.2 mg; 0.705 mmol), ε-caprolactone (ε-CL) (2735 μL; 35 equiv; 24.7 mmol), and trimethylene carbonate (TMC) (2520 mg; 35 equiv; 24.7 mmol). Traces of water were removed by dissolving the solids in anhydrous toluene (ca. 50 mL) followed by concentration in vacuo; this was done twice. Under argon, the dried reagents were redissolved in dry dichloromethane (DCM) (150 mL) while stirring and methane sulfonic acid (MSA) was added (160 μL; 0.1 equiv with respect to ε-CL). The reaction was kept at room temperature for ∼24 h until there was no evidence of residual monomer from the ^{1}H NMR spectra. After completion of the reaction, confirmed by ^{1}H NMR, the reaction mixture was diluted using DCM. The organic phase was washed with saturated $NaHCO_3$ (aq.) followed by a water wash and finally a brine wash. The remaining water from the organic phase was removed using Na_2SO_4 (5−10 min), and the mixture was then filtered and concentrated in vacuo. An oily colorless product was collected. The remaining oil was lyophilized from 1,4-dioxane for 2 days to yield a waxy oil (92% yield, Đ = 1.22). Both purity and copolymer composition were confirmed using ^{1}H NMR (Figure S1a). Composition was calculated using the protons of 1 kDa PEG (3.62−3.68 ppm), terminal methyl unit (s, 3.38 ppm), TMC CH_2 (m 1.89−2.11 ppm), εCL CH_2 (m, 1.33−1.48 ppm), εCL 2× CH_2 (m, 1.54−1.76 ppm), εCL 2× CH_2 (m, 2.25−2.40 ppm), and 2× CH_2 TMC + CH_2 εCL (4.01−4.36 ppm).

Preparation of Azide-Poly(Ethylene Glycol)$_{66}$-*Block*-Poly[(ε-Caprolactone)$_{36}$-*Gradient*-(Trimethylene Carbonate)$_{34}$] (Azide-PEG-p(CL-TMC)). The same protocol as described for PEG-p(CL-TMC) was used. In short, macroinitiator monoazide-PEG (M_n ∼3000 g/mol), ε-CL (35 equiv), TMC (35 equiv), and MSA (0.1 equiv with respect to ε-CL) were used to synthesize block copolymer azide-PEG_{66}-p(CL_{35}-TMC_{35}) (78% yield, Đ = 1.20). Both purity and copolymer composition were confirmed using ^{1}H NMR (Figure S1b). Composition was calculated using the protons of 3 kDa PEG (3.62−3.68 ppm), TMC CH_2 (m 1.89−2.11 ppm), εCL CH_2 (m, 1.33−1.48 ppm), εCL 2× CH_2 (m, 1.54−1.76 ppm), εCL 2× CH_2 (m, 2.25−2.40 ppm), and 2× CH_2 TMC + CH_2 εCL (4.01−4.36 ppm).

Preparation of Amine-Poly(Ethylene Glycol)$_{22}$-*Block*-Poly-[(ε-Caprolactone)$_{38}$-*Gradient*-(Trimethylene Carbonate)$_{36}$] (Amine-PEG-p(CL-TMC)). The same protocol as described for PEG-p(CL-TMC) was used. In short, macroinitiator monoamine-PEG (M_n ∼1000 g/mol), ε-CL (35 equiv), TMC (35 equiv), and MSA (0.3 equiv with respect to ε-CL) were used to synthesize block copolymer amine-PEG_{22}-p(CL_{38}-TMC_{36}) (83% yield, Đ = 1.38). Both purity and copolymer composition were confirmed using ^{1}H NMR (Figure S1c). Composition was calculated using the protons of 1 kDa PEG (3.62−3.68 ppm), TMC CH_2 (m 1.89−2.11 ppm), εCL CH_2 (m, 1.33−1.48 ppm), εCL 2× CH_2 (m, 1.54−1.76 ppm), εCL 2× CH_2 (m, 2.25−2.40 ppm), and 2× CH_2 TMC + CH_2 εCL (4.01−4.36 ppm).

Fluorescent Labeling of PEG-p(CL-TMC) with BODIPY-FL Carboxylic Acid (PEG-p(CL-TMC)-BODIPY). A 10 mL single-neck round-bottom flask was charged with polymer PEG-p(CL-TMC), BODIPY-FL-carboxylic acid (1.5 equiv with respect to the polymer), 4-dimethylaminopyridine (0.5 equiv with respect to fluorescent dye), and 1-ethyl-3-(3-dimethylaminopropyl)carbodiimide (10 equiv with respect to acid). This mixture was dissolved in 4 mL of precooled DMF/DCM (4:1) while stirring (using an ice bath with saturated NaCl, ∼−20 °C). The reaction mixture was shielded from light.

https://doi.org/10.1021/acs.biomac.1c00985
Biomacromolecules 2021, 22, 4422−4433

Table 1. Characteristics of Polymersomes Used in This Study[a]

polymersome variant	mean [Fc] (μg/mL)	conjugation efficiency (%)	mean [CpG] (μg/mL)	conjugation efficiency (%)	size (nm)	PDI	mean ζ-potential ± SD (mV)
Ps					129	0.098	−12.30 ± 0.07
Ps-Fc	373	35			111	0.222	−7.15 ± 0.61
Ps-CpG			169	44	89	0.148	−36.70 ± 0.21
Ps^+					103	0.145	+22.60 ± 0.42
Ps^++CpG			500		202[b]	0.562[b]	−31.10 ± 5.39[b]
Ps-Fc-CpG	340	33	227	60	88	0.158	−42.50 ± 1.84

[a]Ps: nonfunctionalized polymersomes; Ps-Fc: polymersomes displaying Fc conjugated to surface; Ps-CpG: polymersomes displaying CpG conjugated to surface; Ps^+: nonfunctionalized positively charged polymersomes; Ps^++CpG: positively charged polymersomes with CpG adsorbed to surface; Ps-Fc-CpG: polymersomes displaying both CpG and Fc fragments conjugated to surface. Fc and CpG concentrations correspond to polymersomes at a polymer concentration of 10 mg/mL, yielding 1.3×10^{11} particles/mL. For visualization purposes, all polymersome variants contained block copolymers, which were fluorescently labeled prior to particle formation. Dynamic light scattering (DLS) measurements were performed at 10× dilution in PBS to determine size and polydispersity index (PDI). For ζ-potential measurements, the samples were diluted 10× in MQ ($n = 3$). [b]Ps^++CpG at 10 mg/mL aggregated during DLS measurements in MQ due to interactions between positively and negatively charged particles. Size and PDI were determined using 100× dilutions in PBS; ζ-potential was determined using 100× dilutions in MQ.

Triethylamine (10 equiv with respect to acid) was added to the cold mixture. After 2 h, the ice bath was removed, and the reaction mixture was allowed to warm up to room temperature overnight.

The reaction mixture was dialyzed for 24 h (3.5 kDa membrane) against DMSO ($V_{DMSO} = 250 \cdot V_{reaction\ mixture}$), and the dialysis medium was replenished four times. After the fourth time, a complete colorless dialysis medium was obtained, while the product in the dialysis membrane remained fluorescent, indicating successful dialysis. Hereafter, the dialysis medium was switched to 1,4-dioxane and left overnight. The purified compound was collected and freeze-dried immediately for 1 day. A dark-red waxy polymer was obtained. Yield ± 84%.

Coupling of DBCO-PEG$_4$-NHS to Fc Fragment (Fc-DBCO). Prior to conjugation, the buffer of the Fc fragment was exchanged to PBS (1×) by means of spin filtration (3 kDa membrane) at 4 °C. DBCO-PEG$_4$-NHS dissolved in dimethyl sulfoxide (3 equiv) was added to the Fc fragment stock ($V_{DBCOStock}/V_{FcStock}$ = 1:40) and incubated at 4 °C while shaking on a thermoshaker overnight (700 rpm). Hereafter, excess DBCO-PEG$_4$-NHS was removed by spin filtration (3 kDa membrane, washed three times) and the sample was refilled to the original volume using PBS (1×). Sample concentration and degree of labeling (DOL) were determined by absorption spectroscopy as described below.

$$\text{Degree of labeling(DOL)} = \frac{[\text{DBCO}]}{[\text{Fc}]}$$

$$\text{A280c Fc (conjugate's corrected absorbance at 280 nm)} = \text{A280} - (\text{A309 x CF DBCO});\ \text{CF DBCO} = 1.089$$

$$\varepsilon 280\ \text{Fc} = \frac{13.50 * \text{Mw Fc}}{10}$$

$$[\text{Fc}] = \frac{\text{A280c Fc}}{\varepsilon 280\ \text{Fc}};\ \varepsilon 280\ \text{Fc} = 67500$$

$$[\text{DBCO}] = \frac{\text{A309 DBCO}}{\varepsilon 309\ \text{DBCO}};\ \varepsilon 309\ \text{DBCO} = 12000$$

Typical Polymersome Formation Procedure. (Azide/amine-)PEG-p(CL-TMC)(-BODIPY) block copolymer was dissolved in poly(ethylene glycol) (molecular weight ~350 g/mol, PEG350) at 10 wt %. Hereafter, the polymer solutions were mixed according to specific conditions needed for the experiment. This mixture (20 μL) was added to a 5 mL flat-bottom glass vial, equipped with a magnetic stir bar (length of the stir bar ≈ inner diameter of the vial), directly next to the stir bar in the middle of the vial. Endotoxin-free PBS (1×, 80 μL) at room temperature was added rapidly to the mixture while stirring at 250 rpm. Directly, a hazy mixture was formed. After 5 min of stirring, PBS (1×) was slowly added to dilute the sample to the concentration needed. Hereafter, the polymersomes were functionalized with Fc and/or CpG (described below). To remove residual PEG350 from nonfunctionalized polymersomes, typically, a 500 μL spin filter (100 kDa membrane) was filled with 100 μL of polymersomes and cooled to 4 °C. The sample was filtered at 3500g at 4 °C for 30 min. This was done four times, adding ~400 μL endotoxin-free PBS (1×) each time. Finally, the samples were diluted to the desired concentration and filtered using a 0.2 μm endotoxin-free filter.

Fc and CpG Conjugation to the Polymersome Surface. Prior to Fc conjugation, Fc fragments were coupled to DBCO (as described above). Fc-DBCO/CpG-DBCO (1.1 equiv, with respect to the amount of azide-PEG-p(CL-TMC) on the outside of the polymersomes, which was estimated to be ~50% of the total amount of azide polymer within the particle) was incubated with the polymersome solution while mixing on a thermoshaker overnight (4 °C, 700 rpm). Hereafter, the sample was purified. Typically, a 500 μL spin filter (100 kDa membrane) was filled with 100 μL of functionalized polymersomes mixture and cooled to 4 °C. The sample was filtered at 3500g at 4 °C for 30 min. This was done four times, adding ~400 μL of endotoxin-free PBS (1×) each time. After the last run, the sample volume was diluted to the original volume to measure the Fc/CpG concentration and conjugation efficiency. Finally, the samples were diluted to the desired concentration and filtered using a 0.2 μm endotoxin-free filter.

Purification effectiveness was assessed by mixing Fc-DBCO/CpG-DBCO with polymersomes containing no clickable handle, i.e., no azide functionality, and exposing the particles to the same reaction conditions and spin filter method. Hereafter, the Fc/CpG concentration was measured resulting in no signal, indicating efficient purification.

CpG Adsorption to the Polymersomes Surface. CpG ODN 2006 was dissolved in endotoxin-free PBS (1×) and slowly added to a suspension of charged polymersomes while stirring at 600 rpm. Finally, the samples were diluted to the desired concentration and filtered using a 0.2 μm endotoxin-free filter.

Determination of the Concentration of Fc Fragment on the Polymersome Surface. Fc fragment concentration and conjugation efficiency were determined by the Pierce BCA Protein Assay on a plate reader. Polymersomes without any modification on the surface were used as blank, and their absorbance values were subtracted from the Fc conjugated polymersomes. The calibration curve of the Fc fragment was correlated to the BSA calibration curve, provided within the kit. Measurements were carried out in duplicate, and mean concentration and conjugation efficiency are given in Table 1.

Conjugation efficiency was calculated as follows

https://doi.org/10.1021/acs.biomac.1c00985
Biomacromolecules 2021, 22, 4422−4433

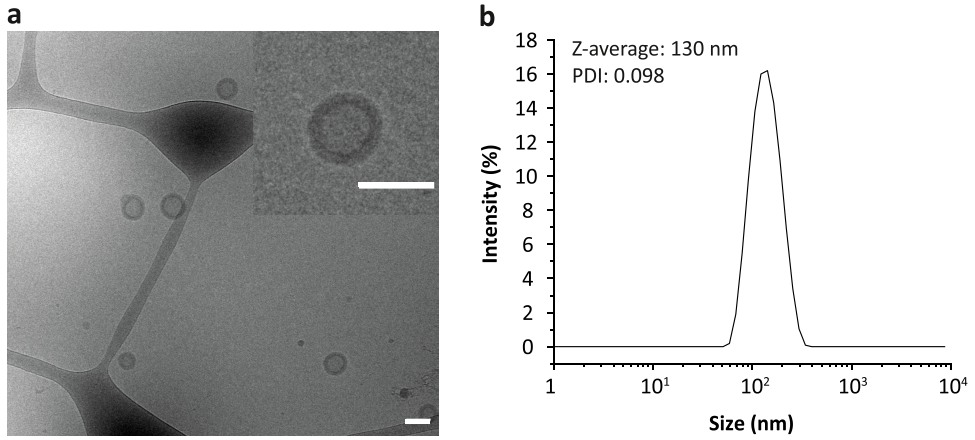

Figure 1. Characterization of typical PEG-p(CL-TMC) polymersomes. (a) Typical cryogenic transmission electron microscopy pictures of PEG-p(CL-TMC) polymersomes, overview and higher-resolution image (inset). Scale bars represent 100 nm. (b) Hydrodynamic size analysis of polymersomes shown in an intensity plot generated by dynamic light scattering (DLS). *Z*-average: intensity-weighted mean hydrodynamic size; PDI: polydispersity index.

$$\text{Conjugation efficiency}(\%) = \frac{[\text{Conjugated Fc}]*100}{[\text{Theoretical maximum Fc on surface polymersome}^*]}$$

*Theoretical maximum was based on the available azide handles exposed on the surface of the polymersome, which was estimated to be ∼50% of the total amount of azide polymer within the particle.

Determination of the Concentration of CpG on the Polymersome Surface. CpG concentration was determined by dissolving the polymersome samples in DMSO (3:1; DMSO/sample) and measuring the absorption at 280 nm on a NanoDrop. Polymersomes without any CpG were used as blank, and their absorbance values were subtracted from the CpG-containing polymersomes. The CpG concentration as well as the conjugation efficiencies are given in Table 1.

Conjugation efficiency was calculated as follows

$$\text{Conjugation efficiency}(\%) = \frac{[\text{Conjugated CpG }]*100}{[\text{Theoretical maximum CpG on surface polymersome}^*]}$$

*Theoretical maximum was based on the available azide handles exposed on the surface of the polymersome, which was estimated to be ∼50% of the total amount of azide polymer within the particle.

Human Leukocyte Isolation. Blood of healthy adult volunteers was collected in vacutainers (BD Vacutainer, Germany) containing Hirudin to prevent coagulation, after providing written informed consent. Leukocytes were obtained by lysing erythrocytes using a freshly prepared ammonium chloride shock buffer (155 mM NH_4Cl; 0.1 mM Na_2EDTA; 10 mM $KHCO_3$) (Merck, Darmstadt, Germany). Briefly, whole blood was incubated for 15 min in ice-cold shock buffer at a 1:9 ratio. Leukocytes were subsequently pelleted by centrifugation (250*g*, 10 min, 4 °C) and washed twice with shock buffer and once with PBS. The cells were finally resuspended in RPMI 1640 Glutamax (Invitrogen) supplemented with 1 mM penicillin/streptomycin (Biowest) and kept on ice.

Leukocyte−Polymersome Interaction Assay. Isolated leukocytes (5×10^5, 100 μL) were plated per well of a sterile 96-well round-bottom plate (Falcon, Corning) and mixed with 5 μL of BODIPY-labeled polymersomes in a cell:particle ratio of 1:5 or 1:50. A polymer amount of 0.385 mg was estimated to correspond to 5×10^9 polymersomes. To block particle uptake, leukocytes were incubated with Cytochalasin D (Sigma) at a final concentration of 10 mM for 15 min at 37 °C, prior to adding polymersomes. The cells were incubated with polymersomes for 30 or 60 min at 37 °C, 250 rpm. Subsequently, the cells were stained with LIVE/DEAD Fixable Dead Cell Stain Kit-Far Red (Invitrogen) according to manufacturer's recommendations and followed by fluorescent labeling of cell markers: CD45-BV510 (clone HI30, BD Biosciences), CD14-PE-Cy7 (clone HCD14, Biolegend), CD66b-BV421 (clone G10F5, BD Biosciences), CD56-PE (clone C5.9, Cytognos, Spain), and CD3-APC-Cy7 (clone SK7, BD Biosciences). Flow cytometry data were collected on a BD LSR II (BD Biosciences) and analyzed using FlowJo 10.2 Software (Figure S1). Dead cells and CD45 negative events were excluded from the data analysis.

Whole Blood Stimulation Assay. Human whole blood was collected as described above, immediately diluted 1:4 in RPMI medium, and mixed with different polymersome variants or soluble CpG. CpG was used at a final concentration of 4 μg/mL. The number of polymersomes between different stimulation conditions deviated based on the CpG concentration in the sample. For polymersome variants lacking CpG, the number of particles in the stimulation was equal to the number of polymersomes used for the polymersome variant with the lowest CpG concentration (Ps-CpG). The cells were stimulated for 24 h at 37 °C, 5% CO_2, after which the culture supernatant was collected and stored at −20 °C for cytokine analysis.

Cytokine Measurements by ELISA. Whole blood stimulation supernatants were analyzed for the level of IL-6 using ELISA kits (Sanquin), performed according to manufacturer's recommendations.

Intracellular Cytokine Analysis by Flow Cytometry. Whole blood stimulations were performed as described above, except that cells were stimulated for 2 h 37 °C, 5% CO_2, followed by 4 h stimulation in the presence of Brefeldin A (BD Bioscience) and Monensin (BD Bioscience) according to manufacturer's recommendations to block cytokine secretion. Subsequently, red blood cell lysis is performed as described above and cells are stained with LIVE/DEAD Fixable Dead Cell Stain Kit-Far Red (Invitrogen) according to manufacturer's recommendations. To allow intracellular cytokine staining, the cells are treated with Cytofix/Cytoperm kit (BD Bioscience) according to manufacturer's recommendations. The following markers were used to identify cell subsets: CD45-BV510 (BD Bioscience), CD3-APC-Cy7 (BD Bioscience), CD14-PeCy7 (Biolegend), and CD66b-BV421 (BD Bioscience). Each sample divided was separately analyzed for the presence of IL-6 (IL-6-PECF594, Clone: MQ2-13A5, BD Bioscience), IL-8 (IL-8-PECF594, clone: G265−8, BD Bioscience), or TNF-α (TNF-α-PECF594, clone: MAB11, BD Bioscience). Flow cytometry data were collected on a BD LSR II and analyzed using FlowJo 10.2 Software (Figure S2). Dead cells and CD45 negative events were excluded from the data analysis.

RESULTS AND DISCUSSION

Polymersome Characterization and Decoration with Fc Fragments. Polymersomes can be assembled from various

https://doi.org/10.1021/acs.biomac.1c00985
Biomacromolecules 2021, 22, 4422−4433

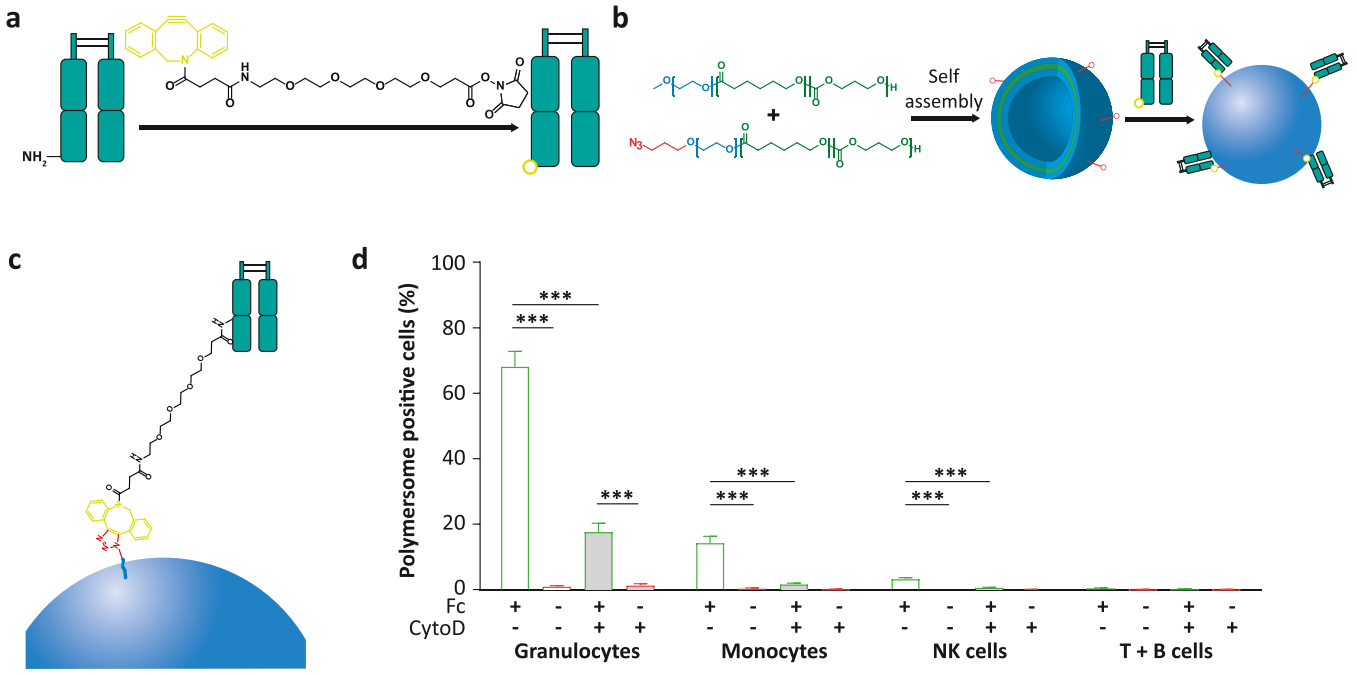

Figure 2. Fc fragment display on the polymersome surface improves particle adhesion to and uptake by immune cells. (a) Purified Fc fragments were labeled with a DBCO group using DBCO-PEG$_4$-NHS, which is reactive with any primary amine of the Fc fragment. (b) PEG-p(CL-TMC) block copolymers with and without azide group were used to induce polymersome formation. Upon the addition of Fc fragments with DBCO-linker, Fc fragments were conjugated to the polymersome surface using the SPAAC reaction. (c) A covalent bond was formed between the azide group on the Ps surface and the DBCO group bound to the Fc fragment. (d) Human leukocytes derived from shocked blood were incubated with polymersomes decorated with or without Fc in a 1:50 ratio for 60 min in the presence or absence of Cytochalasin D (CytoD), an actin polymerization inhibitor, blocking cellular uptake. After incubation, the cells were stained with an antibody panel and analyzed by flow cytometry to distinguish the different cell types. Data are presented as percentage of viable cells positive for polymersomes. Error bars represent the standard error of the mean of five independent experiments with cells from different donors. Statistical analysis was performed using a repeated-measures one-way ANOVA with 95% confidence intervals and Bonferroni correction, comparing polymersomes with and without Fc, and conditions with and without CytoD. Analysis is done for each cell type separately. ***$p < 0.001$.

amphiphilic block copolymers. Here, poly(ethylene glycol)-*block*-poly[(ε-caprolactone)-*gradient*-(trimethylene carbonate)] (PEG-p(CL-TMC)) (Figure S3a) was chosen as the building block for the bilayered vesicle. It has been shown by others that PEG-p(CL-TMC) reproducibly self-assembles into robust particles of ∼100 nm in diameter;[3,5,48] however, at present, its suitability as a vaccine scaffold and its interaction with human immune cells have not yet been evaluated. The base polymer for the formation of biodegradable polymersomes, block copolymer PEG$_{22}$-p(CL$_{35}$-TMC$_{35}$), was synthesized via cationic ring-opening polymerization, resulting in a polymer with a dispersity of Đ = 1.22. Upon self-assembly by direct hydration, well-defined polymersomes with a typical hydrodynamic diameter of 100−130 nm and a low polydispersity index (PDI = 0.098) were formed (Ps; Figure 1a,b and Table 1).

The conjugation of Fc fragments to the surface of the polymersome was achieved using a DBCO-azide SPAAC reaction (copper-free strain-promoted alkyne-azide click chemistry). To this end, azide-PEG-p(CL-TMC) was synthesized with a dispersity of Đ = 1.20. A longer PEG chain compared to the base polymer, 3.0 kDa versus 1.0 kDa, was used to facilitate conjugation between the Fc fragment and the vesicle. Azide-PEG-p(CL-TMC) was blended in at 5 wt % with the base polymer and successfully assembled into polymersomes, demonstrating that the larger azide-containing PEG chain did not interfere with polymersome formation (Figure S3b,c).

The Fc fragment was modified with a DBCO handle to enable conjugation to the azide-functionalized polymersomes (Figure 2a−c). This handle was introduced by incubating Fc fragments with DBCO-PEG$_4$-NHS, reactive with any primary amine of the Fc fragment (Figure 2a). A degree of labeling of ∼1, i.e., approximately one linker per Fc molecule, was chosen to prevent cross-linking and, consequently, polymersome aggregation. Hereafter, the Fc-DBCO fragment was incubated with 5 wt % azide-functionalized polymersomes, resulting in conjugation of the Fc fragments to the polymersome surface, with a conjugation efficiency of 35% (Ps-Fc; Figure 2b,c and Table 1). Following Fc fragment conjugation, a small change in ζ-potential was observed, −7.15 mV, compared to −12.3 mV, for nonfunctionalized polymersomes due to the introduction of the Fc fragments' charge to the surface of the polymersome (Table 1).

Display of Fc Fragments on the Polymersome Surface Mainly Improves Particle Uptake by Human Granulocytes. To evaluate whether polymersomes displaying human Fc fragments could be used to improve the delivery of polymersomes to immune cells, the interaction between these particles and human leukocytes was assessed using flow cytometry (Figures 2d and S4).

Following lysis of red blood cells, human leukocytes were incubated with Ps-Fc to determine the optimal incubation length and cell:polymersome ratio. After a 30 min incubation at a cell:polymersome ratio of ∼1:50, a significant proportion of granulocytes and monocytes had bound Ps-Fc (Figure S4a).

https://doi.org/10.1021/acs.biomac.1c00985
Biomacromolecules 2021, 22, 4422−4433

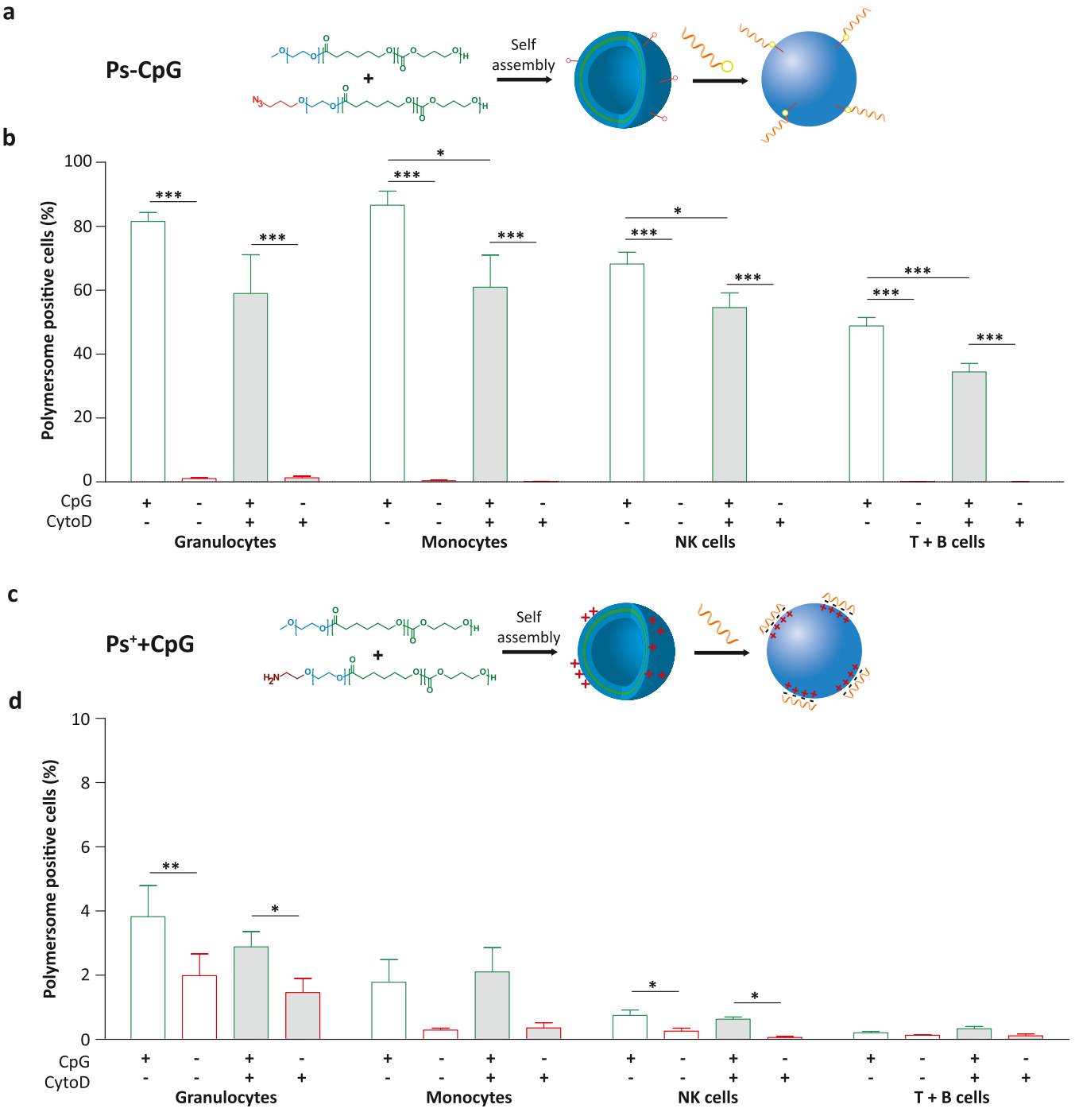

Figure 3. CpG conjugation to the polymersome surface strongly enhances the interaction with human immune cells. (a, c) Schematic representation of polymersomes and (b, d) human leukocytes derived from shocked blood were incubated with polymersomes decorated with or without CpG in a 1:50 ratio for 60 min in the presence or absence of Cytochalasin D (CytoD), an actin polymerization inhibitor, blocking cellular uptake. After incubation, the cells were stained with an antibody panel and analyzed by flow cytometry to distinguish the different cell types. Data are presented as a percentage of viable cells positive for polymersomes. (a) PEG-p(CL-TMC) block copolymers with and without azide groups were used for polymersome formation. Upon the addition of CpG with a DBCO handle, CpG was covalently linked to the polymersome surface using the SPAAC reaction (Ps-CpG). (b) Impact of CpG conjugation to the polymersome surface on the interactions with leukocytes. (c) PEG-p(CL-TMC) block copolymers with and without amines were used for polymersome formation. CpG was subsequently adsorbed to the polymersome surface by electrostatic interactions (Ps^++CpG). (d) Impact of CpG adsorption to positively charged polymersome on the interactions with leukocytes. Error bars represent the standard error of the mean of five independent experiments with cells from different donors. Statistical analysis was performed using a repeated-measures one-way ANOVA with 95% confidence intervals and Bonferroni correction, comparing polymersomes with and without CpG, and conditions with and without CytoD. Analysis is done for each cell type separately. *$p < 0.05$; **$p < 0.01$; ***$p < 0.001$.

Most granulocytes (80%) became positive for Ps-Fc after 30 min, which did not further increase after 60 min. The interaction of Ps-Fc with monocytes increased between 30 min (35%) and 60 min (60%). Similarly, Natural Killer (NK) cells

https://doi.org/10.1021/acs.biomac.1c00985
Biomacromolecules 2021, 22, 4422−4433

showed increased Ps-Fc positivity over time, ranging from 10% at 30 min to 20% at 60 min. No significant interaction of Ps-Fc with T and/or B cells was observed. Of note, the addition of Cytochalasin D (CytoD), which inhibits actin polymerization and thereby blocks cellular uptake, significantly reduced the interactions of Ps-Fc with monocytes and NK cells, but only after 60 min of incubation. Although CytoD had no effect on the percentage of Ps-Fc-positive granulocytes (Figure S4a), a lower mean fluorescence intensity (MFI) was observed (Figure S4b). When using a cell:polymersome ratio of 1:5 (Figure S4c,d), a lower percentage of Ps-Fc-positive leukocytes and a lower MFI were observed compared to the 1:50 ratio.

Based on these results, a cell:polymersome ratio of 1:50 was incubated for 60 min to compare the interaction of Fc-positive and Fc-negative polymersomes with human immune cells (Figure 2d). Especially granulocytes, well known for their capacity to phagocytose pathogens,[49] and also monocytes and NK cells became positive for polymersomes following incubation with Ps-Fc, with 70, 20, and 5% of the cells being Ps-Fc-positive, respectively. In contrast, nonfunctionalized polymersomes did not show significant interaction with human immune cells. In addition, no interaction of polymersomes with or without Fc was detected with T and B cells. In the presence of CytoD, lower percentages of cells positive for Ps-Fc were obtained for monocytes, granulocytes, and NK cells (Figure 2d). Together, these results indicate that polymersome decoration with Fc fragments substantially improves the adhesion and uptake of these particles by immune cells, as was previously shown for other Fc-decorated nanoparticles.[21,22,29,30] It should be noted, however, that the Fc fragments used here were purified from human serum, thus representing the natural distribution of Fc fragments in the circulation. These Fc fragments can interact with a wide variety of FcRs with different affinities. These different interactions have distinct intracellular consequences, influenced by the presence of an immunoreceptor tyrosine-based activation or inhibition motif, ITAM, and ITIM, respectively.[50] As granulocytes, monocytes, and NK cells each express a variety of different FcRs, it is conceivable that the Fc fragment display on the polymersome surface mediates particle uptake via multiple FcR subtypes.[50] Targeting a specific type of FcR could represent an elegant strategy to increase targeting specificity.[22,29]

Polymersome Surface Functionalization via Conjugation or Adsorption of CpG. To explore the impact of CpG-mediated targeting, polymersomes with surface displayed CpG were produced. CpG was conjugated to the polymersome surface in a manner similar to the Fc fragments, using the SPAAC reaction (Ps-CpG; Figure 3a). The conjugation of CpG-DBCO to the polymersome surface, containing 15 wt % azide polymer, was analyzed by absorption spectroscopy, resulting in a coupling efficiency of 44% (Table 1). Due to the high negative charge of CpG, the ζ-potential of the polymersome shifted significantly compared to Ps, from −12.3 to −36.7 mV (Table 1), confirming surface functionalization of the polymersome with CpG.

Alternatively, we adsorbed the negatively charged CpG to the surface of positively charged polymersomes (Ps^++CpG; Figure 3c). To introduce a positive charge, amine-PEG-p(CL-TMC) was synthesized by cationic ring-opening polymerization (Đ = 1.38). The content of the amine-containing polymer was kept at 50 wt % for all experiments, resulting, upon direct hydration, in vesicles with a size of ∼100 nm (Ps^+; Figure S5a,b) with a significantly higher ζ-potential, +22.6 mV, compared to the Ps with a ζ-potential of −12.3 mV (Table 1). Because of the strong interaction between particles and CpG and, consequently, concentration-dependent coagulation of the particles, DLS analysis of Ps^++CpG was performed using a 100-fold dilution in PBS and revealed a particle size of ∼202 nm. A large shift in ζ-potential was detected after the addition of CpG to positively charged polymersomes, +22.6 to −15 mV, indicating coating of the surface with the adjuvant (Table 1 and Figure S5c).

Conjugation of CpG to the Polymersome Surface Strongly Enhances the Interaction with a Wide Variety of Human Leukocytes. To study the impact of CpG decoration on the interaction of polymersomes with human leukocytes, we repeated the flow cytometry assay as described above for Ps-Fc. Immune cells were incubated with different polymersome variants at a ratio of 1:50 for 60 min, in the presence or absence of CytoD, followed by flow cytometry analysis (Figure 3b,d).

Conjugation of CpG to the polymersome surface resulted in a marked and significant increase in the percentage of polymersome-positive cells compared to nonfunctionalized polymersomes (Figure 3b). Of each of the assessed cell populations, 50−90% of the cells were positive for Ps-CpG, whereas hardly any polymersome-positive cells were measured when nonfunctionalized polymersomes were used. Adding CytoD resulted in only a minor decrease in the percentage of polymersome-positive cells, with ∼50% of the cells per leukocyte subset still demonstrating polymersome binding after incubation with Ps-CpG. This may indicate that the majority of the cells became polymersome-positive due to particle adhesion or actin-independent uptake. The internalization of CpG displaying particles could potentially be mediated by interaction with TLR-9, as besides its intracellular localization, it is also been found at the cell surface.[51] In addition, DEC205, a cell surface C-type lectin receptor family member, and scavenging receptors have been shown to bind CpG and are expressed by a wide range of cell types.[18,52−54] Targeting DEC205 on dendritic cells has shown to induce the enhancement of antigen presentation by these cells and might therefore be an interesting target for vaccine development.[55−57] As engagement of DEC205 results in internalization via clathrin-coated pits,[18,57] this may explain the limited impact of CytoD, inhibiting actin polymerization, on the percentage of polymersome-positive cells in the presence of Ps-CpG.

In contrast to conjugated CpG (Ps-CpG), incubation of polymersomes with adsorbed CpG (Ps^++CpG) with human leukocytes resulted in only up to 4% of polymersome-positive cells (Figure 3d), which could be explained by the loss of CpG from the particle during the experiment. Thus, decorating polymersomes with CpG can be used to improve their interaction with human immune cells, as was previously shown using other nanoparticles,[37−44,58] but requires CpG to be covalently bound to the polymersome surface.

Bimodal Targeting of Polymersomes to Human Immune Cells Is Mostly Dependent on CpG Conjugation. As we found that both Fc fragment and CpG conjugation to the polymersome surface can significantly strengthen the interaction of polymersomes with human immune cells, we subsequently explored whether their combined use could further improve the targeting of polymersomes to human leukocytes (Figure 4a). To this end, polymersomes displaying

https://doi.org/10.1021/acs.biomac.1c00985
Biomacromolecules 2021, 22, 4422−4433

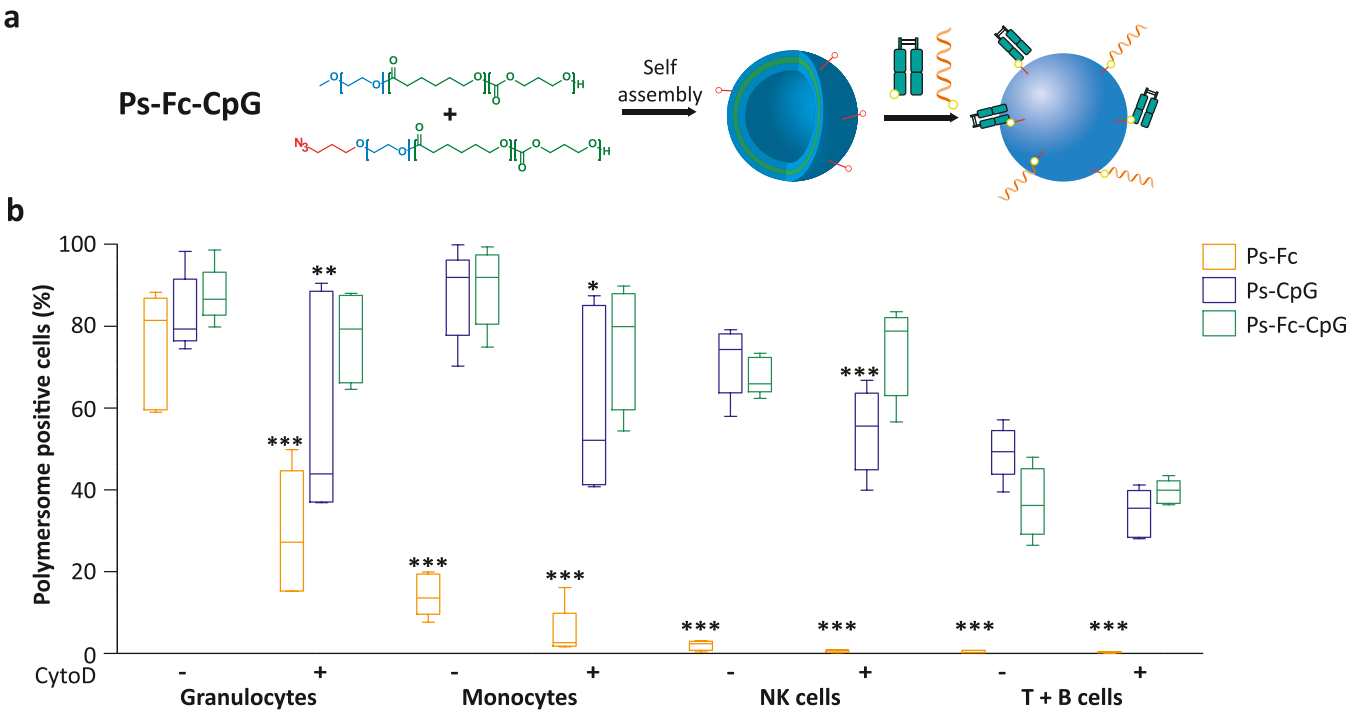

Figure 4. Interaction of Ps-Fc-CpG with human leukocytes is mainly determined by CpG conjugation. (a) Schematic representation of polymersomes decorated with Fc and CpG using the SPAAC reaction (Ps-Fc-CpG). (b) Impact of Fc and CpG conjugation to the polymersome surface on the interaction with leukocytes (n = 5). Human leukocytes derived from shocked blood were incubated with polymersomes decorated with or without Fc and CpG in a 1:50 ratio for 60 min in the presence or absence of Cytochalasin D (CytoD), an actin polymerization inhibitor, blocking cellular uptake. After incubation, cells were stained with an antibody panel and analyzed by flow cytometry to distinguish the different cell types. Data are presented as a percentage of viable cells positive for polymersomes. Statistical analysis was performed using a repeated-measures one-way ANOVA with 95% confidence intervals and Bonferroni correction, comparing Ps-Fc-CpG to Ps-Fc and Ps-CpG. Analysis is done for each cell type and the with and without CytoD condition separately. *p < 0.05; **p < 0.01; ***p < 0.001.

both Fc-DBCO and CpG-DBCO were made using 20 wt % azide polymer, and sequential conjugation of Fc fragments and CpG was performed, i.e., first, Fc-DBCO conjugation, followed by CpG-DBCO conjugation, with efficiencies of 33 and 60%, respectively (Ps-Fc-CpG; Table 1). Cryogenic transmission electron microscopy (Cryo-TEM) analysis demonstrated that the bilayered nature of the polymersomes remained intact after the conjugation of both compounds (Figure S6a), and DLS measurements confirmed the formation of reproducibly sized particles (Figure S6b). Interestingly, none of the chemical modifications included in the present study did significantly affect the size or morphology of the polymersomes, underscoring their robustness and versality and making them a highly suitable nanocarrier.[45,46,59−61]

Analysis of the interaction of Ps-Fc-CpG with human leukocytes in comparison to Ps-Fc and Ps-CpG revealed that Ps-CpG and Ps-Fc-CpG gave highly similar results (Figure 4b), whereas Ps-Fc induced significantly lower percentages of polymersome-positive cells. These data strongly suggest that CpG conjugation contributed significantly more to cell−polymersome interactions than Fc fragment conjugation. Of note, in the presence of CytoD, the percentage of polymersome-positive cells was almost always higher for Ps-Fc-CpG than Ps-CpG (Figure 4b).

Decoration with Both CpG and Fc Fragments Enhances the Immune Stimulatory Capacity of Polymersomes. Having identified that CpG conjugation and, to a lesser extent, Fc conjugation enhance the cellular targeting of polymersomes, we then investigated their capacity to induce a proinflammatory cytokine response when incubated with whole blood (Figure 5).

Following a 24 h stimulation, the interleukin (IL)-6 level in the culture supernatant was determined (Figure 5a). In line with the absence of detectable phagocytosis of nonfunctionalized PEG-p(CL-TMC) polymersomes, these particles did not induce detectable IL-6 levels, confirming the previously described inert properties of PEGylated particles.[15,62] Conversely, Ps-Fc and Ps-CpG triggered a slightly elevated IL-6 response compared to stimulation with mock or Ps. Moreover, Ps-Fc-CpG induced significantly higher IL-6 levels than Ps-Fc and Ps-CpG (Ps-Fc versus Ps-Fc-CpG: p = 0.0013, fold-increase: 9.5; Ps-CpG versus Ps-Fc-CpG: p = 0.0265, fold-increase: 5.4) (Figure 5a).

To determine whether the bimodal targeting has a synergistic rather than a cumulative effect, the IL-6 level after stimulation with Ps-Fc-CpG was divided by the sum of IL-6 levels after stimulation with Ps-Fc and Ps-CpG (Figure 5b). This ratio was >1 for all donors (p-value = 0.0313), suggesting a mild synergistic effect of polymersomes displaying both Fc fragments and CpG on the IL-6 response. Thus, while the bimodal targeting approach did not further improve the quantity of cell−particle interactions compared to polymersomes decorated with only CpG (Figure 4b), the functional cytokine response was increased. The large variation in cytokine response between donors could possibly be explained by differences in expression levels of various Fc and CpG receptors, which have different intracellular consequences.

To gain insight into the cells responsible for cytokine production, we performed whole blood stimulations for 6 h

https://doi.org/10.1021/acs.biomac.1c00985
Biomacromolecules 2021, 22, 4422−4433

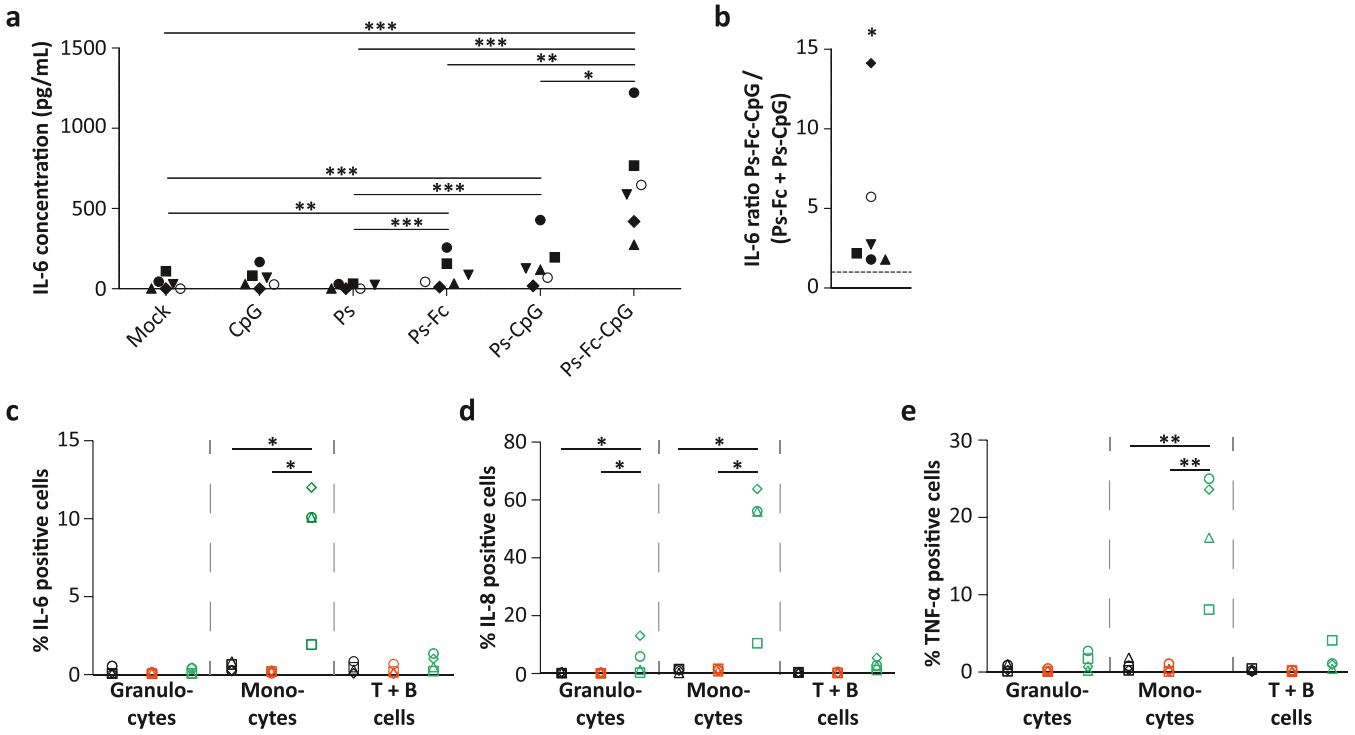

Figure 5. Fc and CpG conjugation to the polymersome surface enhances the proinflammatory cytokine response in a human whole blood stimulation assay. Human whole blood was stimulated with different polymersome variants or soluble CpG at a final concentration of 4 μg CpG/mL. In case polymersomes did not contain CpG, the same amount of polymersomes was used as required for the polymersome variant with the lowest CpG concentration. (a) IL-6 levels (n = 6) in supernatant after a 24 h stimulation with different polymersome variants measured using ELISA. Detection limit is 2.0 pg/mL. (b) The synergy between Fc fragment and CpG display on the polymersome surface was calculated by dividing the IL-6 response to Ps-Fc-CpG shown in (a) by the sum of the responses to Ps-Fc and Ps-CpG. The dotted line indicates a ratio of 1. (c−e) Whole blood was stimulated with mock (black), Ps (red), or Ps-Fc-CpG (green) (n = 4) for a total of 6 h, of which 4 h in the presence of cytokine secretion blocking reagents. Leukocytes from shocked stimulated whole blood were stained with an antibody panel to distinguish the different cell types and to detect IL-6, IL-8, or TNF-α by flow cytometry. Data are presented as a percentage of viable cells positive for IL-6 (c), IL-8 (d), or TNF-α (e). Each symbol represents a donor. Statistical analysis was performed using a repeated-measures one-way ANOVA on log 10 transformed data with Bonferroni correction and 95% confidence intervals. The significance of the synergy was calculated by comparing the IL-6 ratios to 1 using a Wilcoxon signed-rank test. *p < 0.05; **p < 0.01; ***p < 0.001.

while blocking cytokine secretion and analyzed the presence of IL-6, IL-8, and TNF-α intracellularly by flow cytometry (Figure 5c−e).[63] In line with the near-absence of IL-6 in the supernatant, we could not detect IL-6, IL-8, or TNF-α intracellularly upon stimulation with Ps. Following stimulation with Ps-Fc-CpG, only monocytes produced a detectable level of IL-6, albeit only 2−12% of monocytes were IL-6-positive (Figure 5c). Similar to IL-6, mainly monocytes were positive for IL-8 and TNF-α upon stimulation with Ps-Fc-CpG (Figure 5d,e). Of note, while not all monocytes did produce a detectable level of cytokines, all monocytes were positive for Ps-Fc-CpG after 6 h (data not shown), suggesting that monocyte subpopulations, which might differ in relative abundance between individuals, respond differently to decorated polymersomes. While T and B cells did not produce any of the measured cytokines upon Ps or Ps-Fc-CpG stimulation, a small percentage of granulocytes produced IL-8 upon stimulation with Ps-Fc-CpG (Figure 5d). This small percentage of granulocytes may contribute to the overall IL-8 response due to the large total number of granulocytes in the circulation. In addition, granulocytes may contribute to adaptive immune responses by transporting and presenting antigens and regulating antigen-specific responses.[64−66] Therefore, the improved targeting of granulocytes by Fc- and/or CpG-decorated polymersomes, as well as monocytes,[67] could potentially improve antigen presentation and subsequent T cell stimulation. Future studies should therefore focus on generating a deeper understanding on the crosstalk between polymersomes and immune cells, e.g., monocyte subsets, and their consequences on a functional level.

Analysis of the presence of IL-6, IL-8, and TNF-α intracellularly upon stimulation with Ps-Fc and Ps-CpG in comparison to Ps-Fc-CpG suggests a beneficial effect of combining both ligands on the proinflammatory response of leukocytes in general, although the percentage of cytokine-positive cells and the type of cytokines induced differ between leukocyte subsets (Figure S7a−c). Although speculative, particle internalization via an FcR may potentially strengthen the response to CpG. Previously, beneficial effects of multitargeting approaches on the immune response have been found when combining CpG with mannose, targeting mannose receptors, on the surface of liposomes,[68] when co-delivering CpG and R848, a TLR-7/8 agonist, using nanoparticles,[69] and when adding mannose to polymersomes containing monophosphoryl lipid A (MPLA), activating TLR-4, and imiquimod, activating TLR-7/8.[46] Notably, despite restricting differences in ligand density between different particles to a minimum, the possibility remains that the elevated cytokine response to Ps-Fc-CpG is also partially due to a more optimal surface density of ligands compared to

https://doi.org/10.1021/acs.biomac.1c00985
Biomacromolecules 2021, 22, 4422−4433

Ps-Fc and Ps-CpG.[70] Further optimization of the Fc fragment and CpG density may enlarge the immune stimulatory capacity of the polymersome.

CONCLUSIONS

The use of nanoparticles as vehicles for drug delivery or vaccine development has emerged over the past decade.[19,71] The effectiveness of delivery depends on the specificity of targeting, determined by the interaction with and activation of cells encountered by the nanoparticle.[14] The PEGylated surface of polymersomes renders these vesicles inert and, consequently, safe. However, this may also affect the success of delivery and thereby limit their use in vaccines. Targeting nanoparticles to APCs using ligands of cell surface receptors is an attractive strategy to improve vaccine responses and protection.[1,19,43] To this end, we decorated polymersomes with CpG and/or Fc fragments and showed that this significantly enhances the interaction of polymersomes with human immune cells. Moreover, CpG and Fc decoration enhance the immune stimulatory capacity of the virtually inert polymersomes. Combined display of both ligands resulted in the highest cytokine responses, underscoring the potential of bimodal-receptor targeting polymersomes. These observations, together with the high versality and biocompatibility of the polymersome platform, highlight its potential as a vaccine delivery vehicle.

ASSOCIATED CONTENT

Supporting Information

The Supporting Information is available free of charge at https://pubs.acs.org/doi/10.1021/acs.biomac.1c00985.

Block copolymer analysis by ^{1}H NMR (Figure S1); gating strategy used in flow cytometry experiments (Figure S2); characterization of base polymer and azide-containing polymersomes (Figure S3); optimization of leukocyte−polymersome interaction assay using Fc fragment-decorated polymersomes (Figure S4); characterization of amine-containing polymersomes and validation of CpG adsorption to the polymersome surface (Figure S5); characterization of polymersomes with Fc fragments and CpG covalently bound to the polymersome surface (Figure S6); Ps-Fc-CpG induces more cells to produce proinflammatory cytokines compared to polymersomes with no or a single ligand (Figure S7) (PDF)

AUTHOR INFORMATION

Corresponding Author

Lucille F. van Beek − *Laboratory of Medical Immunology, Radboud Institute for Molecular Life Sciences, Radboud University Medical Center, 6525 GA Nijmegen, The Netherlands; Radboud Center for Infectious Diseases, Radboud University Medical Center, 6525 GA Nijmegen, The Netherlands;* orcid.org/0000-0002-7126-2580; Phone: +31 (0)24 3614656; Email: Lucille.vanbeek@radboudumc.nl

Authors

Pascal L. W. Welzen − *Department of Biomedical Engineering, Institute for Complex Molecular Systems (ICMS), Eindhoven University of Technology, 5612 AZ Eindhoven, The Netherlands*

Lisa U. Teufel − *Laboratory of Medical Immunology, Radboud Institute for Molecular Life Sciences, Radboud University Medical Center, 6525 GA Nijmegen, The Netherlands; Radboud Center for Infectious Diseases, Radboud University Medical Center, 6525 GA Nijmegen, The Netherlands*

Irma Joosten − *Laboratory of Medical Immunology, Radboud Institute for Molecular Life Sciences, Radboud University Medical Center, 6525 GA Nijmegen, The Netherlands*

Dimitri A. Diavatopoulos − *Laboratory of Medical Immunology, Radboud Institute for Molecular Life Sciences, Radboud University Medical Center, 6525 GA Nijmegen, The Netherlands; Radboud Center for Infectious Diseases, Radboud University Medical Center, 6525 GA Nijmegen, The Netherlands*

Jan van Hest − *Department of Biomedical Engineering, Institute for Complex Molecular Systems (ICMS), Eindhoven University of Technology, 5612 AZ Eindhoven, The Netherlands;* orcid.org/0000-0001-7973-2404

Marien I. de Jonge − *Laboratory of Medical Immunology, Radboud Institute for Molecular Life Sciences, Radboud University Medical Center, 6525 GA Nijmegen, The Netherlands; Radboud Center for Infectious Diseases, Radboud University Medical Center, 6525 GA Nijmegen, The Netherlands*

Complete contact information is available at: https://pubs.acs.org/10.1021/acs.biomac.1c00985

Author Contributions

‖L.F.v.B., P.L.W.W., J.v.H., and M.I.d.J. contributed equally to this work.

Notes

The authors declare no competing financial interest.

ACKNOWLEDGMENTS

This study was supported by "NWO TTW Perspectief Programma", "A technology center for Bacterial Vaccines (BacVactory)".

REFERENCES

(1) Messager, L.; Gaitzsch, J.; Chierico, L.; Battaglia, G. Novel aspects of encapsulation and delivery using polymersomes. *Curr. Opin. Pharmacol.* **2014**, *18*, 104−111.

(2) Rideau, E.; Dimova, R.; Schwille, P.; Wurm, F. R.; Landfester, K. Liposomes and polymersomes: a comparative review towards cell mimicking. *Chem. Soc. Rev.* **2018**, *47*, 8572−8610.

(3) van Oppen, L. M. P. E.; Abdelmohsen, L. K. E. A.; van Emst-de Vries, S. E.; Welzen, P. L. W.; Wilson, D. A.; Smeitink, J. A. M.; Koopman, W. J. H.; Brock, R.; Willems, P. H. G. M.; Williams, D. S.; van Hest, J. C. M. Biodegradable synthetic organelles demonstrate ROS shielding in human-complex-I-deficient fibroblasts. *ACS Cent. Sci.* **2018**, *4*, 917−928.

(4) Discher, D. E.; Ahmed, F. Polymersomes. *Annu. Rev. Biomed. Eng.* **2006**, *8*, 323−341.

(5) Sui, X.; Kujala, P.; Janssen, G.-J.; de Jong, E.; Zuhorn, I. S.; van Hest, J. C. M. Robust formation of biodegradable polymersomes by direct hydration. *Polym. Chem.* **2015**, *6*, 691−696.

(6) Yi, S.; Allen, S. D.; Liu, Y. G.; Ouyang, B. Z.; Li, X.; Augsornworawat, P.; Thorp, E. B.; Scott, E. A. Tailoring nanostructure morphology for enhanced targeting of dendritic cells in atherosclerosis. *ACS Nano* **2016**, *10*, 11290−11303.

(7) Anajafi, T.; Mallik, S. Polymersome-based drug-delivery strategies for cancer therapeutics. *Ther. Delivery* **2015**, *6*, 521−534.

(8) Iyisan, B.; Kluge, J.; Formanek, P.; Voit, B.; Appelhans, D. Multifunctional and dual-responsive polymersomes as robust nanocontainers: design, formation by sequential post-Conjugations, and pH-controlled drug release. *Chem. Mater.* **2016**, *28*, 1513−1525.
(9) Brinkhuis, R. P.; Rutjes, F. P. J. T.; van Hest, J. C. M. Polymeric vesicles in biomedical applications. *Polym. Chem.* **2011**, *2*, 1449−1462.
(10) Dieu, L. H.; Wu, D.; Palivan, C. G.; Balasubramanian, V.; Huwyler, J. Polymersomes conjugated to 83-14 monoclonal antibodies: in vitro targeting of brain capillary endothelial cells. *Eur. J. Pharm. Biopharm.* **2014**, *88*, 316−324.
(11) Zou, T.; Dembele, F.; Beugnet, A.; Sengmanivong, L.; Trepout, S.; Marco, S.; de Marco, A.; Li, M.-H. Nanobody-functionalized PEG-b-PCL polymersomes and their targeting study. *J. Biotechnol.* **2015**, *214*, 147−155.
(12) Lee, J. S.; Feijen, J. Polymersomes for drug delivery: design, formation and characterization. *J. Controlled Release* **2012**, *161*, 473−483.
(13) Meeuwissen, S. A.; Debets, M. F.; van Hest, J. C. M. Copper-free click chemistry on polymersomes: pre- vs. post-self-assembly functionalisation. *Polym. Chem.* **2012**, *3*, 1783−1795.
(14) Brito, L. A.; O'Hagan, D. T. Designing and building the next generation of improved vaccine adjuvants. *J. Controlled Release* **2014**, *190*, 563−579.
(15) Suk, J. S.; Xu, Q.; Kim, N.; Hanes, J.; Ensign, L. M. PEGylation as a strategy for improving nanoparticle-based drug and gene delivery. *Adv. Drug Delivery Rev.* **2016**, *99*, 28−51.
(16) Underhill, D. M.; Ozinsky, A. Phagocytosis of microbes: complexity in action. *Annu. Rev. Immunol.* **2002**, *20*, 825−852.
(17) Moon, J. J.; Huang, B.; Irvine, D. J. Engineering nano- and microparticles to tune immunity. *Adv. Mater.* **2012**, *24*, 3724−3746.
(18) Molino, N. M.; Neek, M.; Tucker, J. A.; Nelson, E. L.; Wang, S.-W. Display of DNA on nanoparticles for targeting antigen presenting cells. *ACS Biomater. Sci. Eng.* **2017**, *3*, 496−501.
(19) Gause, K. T.; Wheatley, A. K.; Cui, J.; Yan, Y.; Kent, S. J.; Caruso, F. Immunological principles guiding the rational design of particles for vaccine delivery. *ACS Nano* **2017**, *11*, 54−68.
(20) Bachmann, M. F.; Jennings, G. T. Vaccine delivery: a matter of size, geometry, kinetics and molecular patterns. *Nat. Rev. Immunol.* **2010**, *10*, 787−796.
(21) Pacheco, P.; White, D.; Sulchek, T. Effects of microparticle size and Fc density on macrophage phagocytosis. *PLoS One* **2013**, *8*, No. e60989.
(22) Adamova, E.; Walsh, M. C.; Gosselin, D. R.; Hale, K.; Preissler, M. T.; Graziano, R. F.; Gosselin, E. J. Enhanced antigen-specific antibody and cytokine responses when targeting antigen to human FcGAMMA receptor type I using an anti-human FcGAMMA receptor type I-streptavidin fusion protein in an adjuvant-free system. *Immunol. Invest.* **2005**, *34*, 417−429.
(23) Heijnen, I. A.; van Vugt, M. J.; Fanger, N. A.; Graziano, R. F.; de Wit, T. P.; Hofhuis, F. M.; Guyre, P. M.; Capel, P. J.; Verbeek, J. S.; van de Winkel, J. G. Antigen targeting to myeloid-specific human Fc gamma RI/CD64 triggers enhanced antibody responses in transgenic mice. *J. Clin. Invest.* **1996**, *97*, 331−338.
(24) White, D. M.; Pellett, S.; Jensen, M. A.; Tepp, W. H.; Johnson, E. A.; Arnason, B. G. Rapid immune responses to a botulinum neurotoxin Hc subunit vaccine through *in vivo* targeting to antigen-presenting cells. *Infect. Immun.* **2011**, *79*, 3388−3396.
(25) Konduru, K.; Bradfute, S. B.; Jacques, J.; Manangeeswaran, M.; Nakamura, S.; Morshed, S.; Wood, S. C.; Bavari, S.; Kaplan, G. G. Ebola virus glycoprotein Fc fusion protein confers protection against lethal challenge in vaccinated mice. *Vaccine* **2011**, *29*, 2968−2977.
(26) Zhang, Y.; Hoppe, A. D.; Swanson, J. A. Coordination of Fc receptor signaling regulates cellular commitment to phagocytosis. *Proc. Natl. Acad. Sci. U.S.A.* **2010**, *107*, 19332−19337.
(27) Bitsaktsis, C.; Iglesias, B. V.; Li, Y.; Colino, J.; Snapper, C. M.; Hollingshead, S. K.; Pham, G.; Gosselin, D. R.; Gosselin, E. J. Mucosal immunization with an unadjuvanted vaccine that targets *Streptococcus pneumoniae* PspA to human Fcgamma receptor type I protects against pneumococcal infection through complement- and lactoferrin-mediated bactericidal activity. *Infect. Immun.* **2012**, *80*, 1166−1180.
(28) Rawool, D. B.; Bitsaktsis, C.; Li, Y.; Gosselin, D. R.; Lin, Y.; Kurkure, N. V.; Metzger, D. W.; Gosselin, E. J. Utilization of Fc receptors as a mucosal vaccine strategy against an intracellular bacterium, *Francisella tularensis*. *J. Immunol.* **2008**, *180*, 5548−5557.
(29) Pridgen, E. M.; Alexis, F.; Kuo, T. T.; Levy-Nissenbaum, E.; Karnik, R.; Blumberg, R. S.; Langer, R.; Farokhzad, O. C. Transepithelial transport of Fc-targeted nanoparticles by the neonatal fc receptor for oral delivery. *Sci. Transl. Med.* **2013**, *5*, No. 213ra167.
(30) Vllasaliu, D.; Alexander, C.; Garnett, M.; Eaton, M.; Stolnik, S. Fc-mediated transport of nanoparticles across airway epithelial cell layers. *J. Controlled Release* **2012**, *158*, 479−486.
(31) Dumont, J. A.; Bitonti, A. J.; Clark, D.; Evans, S.; Pickford, M.; Newman, S. P. Delivery of an erythropoietin-Fc fusion protein by inhalation in humans through an immunoglobulin transport pathway. *J. Aerosol Med.* **2005**, *18*, 294−303.
(32) Kumar, S.; Sunagar, R.; Gosselin, E. J. Preclinical efficacy of a trivalent human FcgammaRI-targeted adjuvant-free subunit mucosal vaccine against pulmonary pneumococcal infection. *Vaccines* **2020**, *8*, No. 193.
(33) Gosselin, E. J.; Bitsaktsis, C.; Li, Y.; Iglesias, B. V. Fc receptor-targeted mucosal vaccination as a novel strategy for the generation of enhanced immunity against mucosal and non-mucosal pathogens. *Arch. Immunol. Ther. Exp.* **2009**, *57*, 311−323.
(34) Comberlato, A.; Paloja, K.; Bastings, M. M. C. Nucleic acids presenting polymer nanomaterials as vaccine adjuvants. *J. Mater. Chem. B* **2019**, *7*, 6321−6346.
(35) Zhang, H.; Gao, X.-D. Nanodelivery systems for enhancing the immunostimulatory effect of CpG oligodeoxynucleotides. *Mater. Sci. Eng., C* **2017**, *70*, 935−946.
(36) Shirota, H.; Klinman, D. M. Recent progress concerning CpG DNA and its use as a vaccine adjuvant. *Expert Rev. Vaccines* **2014**, *13*, 299−312.
(37) de Titta, A.; Ballester, M.; Julier, Z.; Nembrini, C.; Jeanbart, L.; van der Vlies, A. J.; Swartz, M. A.; Hubbell, J. A. Nanoparticle conjugation of CpG enhances adjuvancy for cellular immunity and memory recall at low dose. *Proc. Natl. Acad. Sci. U.S.A.* **2013**, *110*, 19902−19907.
(38) Diwan, M.; Elamanchili, P.; Cao, M.; Samuel, J. Dose sparing of CpG oligodeoxynucleotide vaccine adjuvants by nanoparticle delivery. *Curr. Drug Delivery* **2004**, *1*, 405−412.
(39) Kuai, R.; Sun, X.; Yuan, W.; Ochyl, L. J.; Xu, Y.; Hassani Najafabadi, A.; Scheetz, L.; Yu, M. Z.; Balwani, I.; Schwendeman, A.; Moon, J. J. Dual TLR agonist nanodiscs as a strong adjuvant system for vaccines and immunotherapy. *J. Controlled Release* **2018**, *282*, 131−139.
(40) Liu, J.; Wang, J.; Zhu, Q.; Yu, C.; Yin, J.; Zheng, L.; Li, A. Mannosylated PEGylated-polyethyleneimine as efficient CpG oligodeoxynucleotide carriers for efficient dendritic cell targeting delivery and activation. *J. Biomed. Nanotechnol.* **2019**, *15*, 1454−1467.
(41) Shirai, S.; Shibuya, M.; Kawai, A.; Tamiya, S.; Munakata, L.; Omata, D.; Suzuki, R.; Aoshi, T.; Yoshioka, Y. Lipid nanoparticles potentiate CpG-oligodeoxynucleotide-based vaccine for Influenza virus. *Front. Immunol.* **2020**, *10*, No. 3018.
(42) Zope, H.; Quer, C. B.; Bomans, P. H.; Sommerdijk, N. A.; Kros, A.; Jiskoot, W. Peptide amphiphile nanoparticles enhance the immune response against a CpG-adjuvanted influenza antigen. *Adv. Healthcare Mater.* **2014**, *3*, 343−348.
(43) Zupančič, E.; Curato, C.; Paisana, M.; Rodrigues, C.; Porat, Z.; Viana, A. S.; Afonso, C. A. M.; Pinto, J.; Gaspar, R.; Moreira, J. N.; Satchi-Fainaro, R.; Jung, S.; Florindo, H. F. Rational design of nanoparticles towards targeting antigen-presenting cells and improved T cell priming. *J. Controlled Release* **2017**, *258*, 182−195.
(44) Takahashi, H.; Misato, K.; Aoshi, T.; Yamamoto, Y.; Kubota, Y.; Wu, X.; Kuroda, E.; Ishii, K. J.; Yamamoto, H.; Yoshioka, Y. Carbonate apatite nanoparticles act as potent vaccine adjuvant delivery vehicles by enhancing cytokine production induced by

https://doi.org/10.1021/acs.biomac.1c00985
Biomacromolecules 2021, 22, 4422−4433

encapsulated cytosine-phosphate-guanine pligodeoxynucleotides. *Front. Immunol.* **2018**, *9*, No. 783.
(45) Lim, J.-W.; Na, W.; Kim, H.-O.; Yeom, M.; Kang, A.; Park, G.; Park, C.; Ki, J.; Lee, S.; Jung, B.; Jeong, H. H.; Park, D.; Song, D.; Haam, S. Co-delivery of antigens and immunostimulants via a polymersome for improvement of antigen-specific immune response. *J. Mater. Chem. B* **2020**, *8*, 5620−5626.
(46) Zhu, D.; Hu, C.; Fan, F.; Qin, Y.; Huang, C.; Zhang, Z.; Lu, L.; Wang, H.; Sun, H.; Leng, X.; Wang, C.; Kong, D.; Zhang, L. Co-delivery of antigen and dual agonists by programmed mannose-targeted cationic lipid-hybrid polymersomes for enhanced vaccination. *Biomaterials* **2019**, *206*, 25−40.
(47) Volpatti, L. R.; Wallace, R. P.; Cao, S.; Raczy, M. M.; Wang, R.; Gray, L. T.; Alpar, A. T.; Briquez, P. S.; Mitrousis, N.; Marchell, T. M.; Sasso, M. S.; Nguyen, M.; Mansurov, A.; Budina, E.; Solanki, A.; Watkins, E. A.; Schnorenberg, M. R.; Tremain, A. C.; Reda, J. W.; Nicolaescu, V.; Furlong, K.; Dvorkin, S.; Yu, S. S.; Manicassamy, B.; LaBelle, J. L.; Tirrell, M. V.; Randall, G.; Kwissa, M.; Swartz, M. A.; Hubbell, J. A. Polymersomes decorated with the SARS-CoV-2 Spike Protein Receptor-Binding Domain elicit robust humoral and cellular Immunity. *ACS Cent. Sci.* **2021**, *7*, 1368−1380.
(48) Mason, A. F.; Yewdall, N. A.; Welzen, P. L. W.; Shao, J.; van Stevendaal, M.; van Hest, J. C. M.; Williams, D. S.; Abdelmohsen, L. K. E. A. Mimicking cellular compartmentalization in a hierarchical protocell through spontaneous spatial organization. *ACS Cent. Sci.* **2019**, *5*, 1360−1365.
(49) Mayadas, T. N.; Cullere, X.; Lowell, C. A. The multifaceted functions of neutrophils. *Annu. Rev. Pathol.: Mech. Dis.* **2014**, *9*, 181−218.
(50) Bruhns, P. Properties of mouse and human IgG receptors and their contribution to disease models. *Blood* **2012**, *119*, 5640−5649.
(51) Eaton-Bassiri, A.; Dillon, S. B.; Cunningham, M.; Rycyzyn, M. A.; Mills, J.; Sarisky, R. T.; Mbow, M. L. Toll-like receptor 9 can be expressed at the cell surface of distinct populations of tonsils and human peripheral blood mononuclear cells. *Infect. Immun.* **2004**, *72*, 7202−7211.
(52) Józefowski, S.; Sulahian, T. H.; Arredouani, M.; Kobzik, L. Role of scavenger receptor MARCO in macrophage responses to CpG oligodeoxynucleotides. *J. Leukocyte Biol.* **2006**, *80*, 870−879.
(53) Lahoud, M. H.; Ahmet, F.; Zhang, J.-G.; Meuter, S.; Policheni, A. N.; Kitsoulis, S.; Lee, C.-N.; O'Keeffe, M.; Sullivan, L. C.; Brooks, A. G.; Berry, R.; Rossjohn, J.; Mintern, J. D.; Vega-Ramos, J.; Villadangos, J. A.; Nicola, N. A.; Nussenzweig, M. C.; Stacey, K. J.; Shortman, K.; Heath, W. R.; Caminschi, I. DEC-205 is a cell surface receptor for CpG oligonucleotides. *Proc. Natl. Acad. Sci. U.S.A.* **2012**, *109*, 16270−16275.
(54) Gursel, M.; Gursel, I.; Mostowski, H. S.; Klinman, D. M. CXCL16 influences the nature and specificity of CpG-induced immune activation. *J. Immunol.* **2006**, *177*, 1575−1580.
(55) Bonifaz, L. C.; Bonnyay, D. P.; Charalambous, A.; Darguste, D. I.; Fujii, S.-I.; Soares, H.; Brimnes, M. K.; Moltedo, B.; Moran, T. M.; Steinman, R. M. *In vivo* targeting of antigens to maturing dendritic cells via the DEC-205 receptor improves T cell vaccination. *J. Exp. Med.* **2004**, *199*, 815−824.
(56) Inaba, K.; Swiggard, W. J.; Inaba, M.; Meltzer, J.; Miryza, A.; Sasagawa, T.; Nussenzweig, M. C.; Steinman, R. U. Tissue distribution of the DEC-205 protein that is detected by the monoclonal antibody NLDC-145: I. Expression on dendritic cells and other subsets of mouse leukocytes. *Cell. Immunol.* **1995**, *163*, 148−156.
(57) Jiang, W.; Swiggard, W. J.; Heufler, C.; Peng, M.; Mirza, A.; Steinman, R. M.; Nussenzweig, M. C. The receptor DEC-205 expressed by dendritic cells and thymic epithelial cells is involved in antigen processing. *Nature* **1995**, *375*, 151−155.
(58) Zhang, H.; Chen, S.; Zhi, C.; Yamazaki, T.; Hanagata, N. Chitosan-coated boron nitride nanospheres enhance delivery of CpG oligodeoxynucleotides and induction of cytokines. *Int. J. Nanomed.* **2013**, *8*, 1783−1793.
(59) Gao, M.; Peng, Y.; Jiang, L.; Qiu, L. Effective intracellular delivery and Th1 immune response induced by ovalbumin loaded in pH-responsive polyphosphazene polymersomes. *Nanomed.: Nanotechnol., Biol. Med.* **2018**, *14*, 1609−1618.
(60) Galan-Navarro, C.; Rincon-Restrepo, M.; Zimmer, G.; Ollmann Saphire, E.; Hubbell, J. A.; Hirosue, S.; Swartz, M. A.; Kunz, S. Oxidation-sensitive polymersomes as vaccine nanocarriers enhance humoral responses against Lassa virus envelope glycoprotein. *Virology* **2017**, *512*, 161−171.
(61) Weber, B.; Kappel, C.; Scherer, M.; Helm, M.; Bros, M.; Grabbe, S.; Barz, M. PeptoSomes for vaccination: combining antigen and adjuvant in polypept(o)ide-based polymersomes. *Macromol. Biosci.* **2017**, *17*, No. 1700061.
(62) Immordino, M. L.; Dosio, F.; Cattel, L. Stealth liposomes: review of the basic science, rationale, and clinical applications, existing and potential. *Int. J. Nanomed.* **2006**, *1*, 297−315.
(63) József, L.; Khreiss, T.; El Kebir, D.; Filep, J. G. Activation of TLR-9 induces IL-8 secretion through peroxynitrite Signaling in human neutrophils. *J. Immunol.* **2006**, *176*, 1195−1202.
(64) Vono, M.; Lin, A.; Norrby-Teglund, A.; Koup, R. A.; Liang, F.; Loré, K. Neutrophils acquire the capacity for antigen presentation to memory CD4(+) T cells *in vitro* and *ex vivo*. *Blood* **2017**, *129*, 1991−2001.
(65) Costa, S.; Bevilacqua, D.; Cassatella, M. A.; Scapini, P. Recent advances on the crosstalk between neutrophils and B or T lymphocytes. *Immunology* **2019**, *156*, 23−32.
(66) Lin, A.; Loré, K. Granulocytes: new members of the antigen-presenting cell family. *Front. Immunol.* **2017**, *8*, No. 1781.
(67) Jakubzick, C. V.; Randolph, G. J.; Henson, P. M. Monocyte differentiation and antigen-presenting functions. *Nat. Rev. Immunol.* **2017**, *17*, 349−362.
(68) Lai, C.; Duan, S.; Ye, F.; Hou, X.; Li, X.; Zhao, J.; Yu, X.; Hu, Z.; Tang, Z.; Mo, F.; Yang, X.; Lu, X. The enhanced antitumor-specific immune response with mannose- and CpG-ODN-coated liposomes delivering TRP2 peptide. *Theranostics* **2018**, *8*, 1723−1739.
(69) Ni, Q.; Zhang, F.; Liu, Y.; Wang, Z.; Yu, G.; Liang, B.; Niu, G.; Su, T.; Zhu, G.; Lu, G.; Zhang, L.; Chen, X. A bi-adjuvant nanovaccine that potentiates immunogenicity of neoantigen for combination immunotherapy of colorectal cancer. *Sci. Adv.* **2020**, *6*, No. eaaw6071.
(70) Noble, J.; Zimmerman, A.; Fromen, C. A. Potent immune stimulation from nanoparticle carriers relies on the interplay of adjuvant surface density and adjuvant mass distribution. *ACS Biomater. Sci. Eng.* **2017**, *3*, 560−571.
(71) Bobbala, S.; Hook, S. Is there an optimal formulation and delivery strategy for subunit vaccines? *Pharm. Res.* **2016**, *33*, 2078−2097.

https://doi.org/10.1021/acs.biomac.1c00985
Biomacromolecules 2021, 22, 4422−4433